

A new OSL dose model to account for post-depositional mixing of sediments

Luke A. Yates^{a,*}, Zach Aandahl^a, Barry W. Brook^a, Zenobia Jacobs^{b,c},
Bo Li^{b,c}, Bruno David^{d,e}, and Richard G. Roberts^{b,c}

^a*ARC Centre of Excellence for Australian Biodiversity and Heritage,*

University of Tasmania, Hobart, Tasmania, Australia.

^b*Centre for Archaeological Science, School of Earth, Atmospheric and Life Sciences,*

University of Wollongong, Wollongong, New South Wales, Australia.

^c*ARC Centre of Excellence for Australian Biodiversity and Heritage,*

University of Wollongong, Wollongong, New South Wales, Australia.

^d*Monash Indigenous Studies Centre, Monash University,*

Clayton, Victoria, Australia.

^e*ARC Centre of Excellence for Australian Biodiversity and Heritage,*

Monash University, Victoria, Australia.

* *Corresponding author. Email: luke.yates@utas.edu.au*

This is a non-peer reviewed preprint that has been submitted to Quaternary Geochronology

Abstract

In applications of optically stimulated luminescence (OSL) dating to unconsolidated sediments, the burial age of a sample of grains is estimated using statistical models of the distribution of the experimentally determined equivalent doses of the grains, together with estimates of the environmental dose rate. For grains that have been vertically mixed after deposition (e.g., due to bioturbation), existing dose models may fail to appropriately account for the complexity of the mixing process, thus producing inaccurate age estimates of the original time of deposition of the ‘native’ grains in any particular sample (usually the quantity of most interest). Here we introduce a new dose model, the asymmetric Laplacian mixture model (ALMM), developed for vertically mixed samples with single-grain dose distributions. The approach is based on a continuous statistical mixture that models the displacement of

grains in both upward and downward directions. The central dose of the native grains in each sediment sample is estimated by the ALMM, as well as the parameters associated with overdispersion of single-grain dose distributions and the (modelled) mixing process. Using Bayesian methodology, we apply the model to two series of vertically contiguous samples collected at the site of Nawarla Gabarnmang in northern Australia. Independent age estimates obtained from radiocarbon dating of charcoal fragments support the OSL ages for the native grains estimated by the ALMM. Moreover, our study includes sensitivity analyses that show the model is robust to variation in the experimental error of the OSL data. The ALMM is introduced in the context of compound Gaussian distributions, a broadly encompassing statistical framework that includes many of the most commonly used dose models. This unifying and accessible perspective on the statistical modelling of dose distributions will support practitioners in selecting an appropriate model for samples affected by post-depositional mixing, and hopefully stimulate further theoretical developments. A new R `rstanosl` package is provided that fits the ALMM and other commonly used dose models using Hamiltonian Monte Carlo methods via the Stan programming language.

Key words: optically stimulated luminescence, single-grain dose distributions, vertical mixing of sediments, Bayesian inference, maximum likelihood estimation, asymmetric Laplacian mixture model.

Introduction

In optically stimulated luminescence (OSL) dating, measurements of the equivalent dose (D_e) are commonly made on individual quartz and potassium-rich feldspar grains using the single-aliquot regenerative-dose (SAR) procedure (Galbraith et al., 1999; Murray and Wintle, 2000). The resulting D_e distributions are then visually examined for any patterns in data that might inform about the processes of sample deposition and post-depositional disturbance, as well as grain-to-grain variations in beta dose rate. These insights are combined with estimates of the spread in D_e values remaining after the measurement uncertainties have been taken into account (termed ‘overdispersion’ and denoted as σ_b by Galbraith et al. (2005)) and considerations of sample context to choose an appropriate statistical model to estimate the D_e value of the population of grains associated with the event of interest. This is most often the burial time of grains that have been deposited and then not moved subsequently by anthropogenic, geological or biological processes. In this paper, we refer to these ‘host’ grains (i.e., those in primary depositional context) as ‘native’ grains.

Frequentist and Bayesian models have been developed for sediment samples thought to consist of native grains that were either well-bleached or partially bleached at the time of deposition (Galbraith et al., 1999; Huntriss, 2008; Galbraith and Roberts, 2012; Combès et al., 2015; Christophe et al., 2018; Li et al., 2022). D_e distributions that consist of grains drawn from multiple discrete dose populations can also be modelled using frequentist and Bayesian methods (e.g., Roberts et al., 2000; Sivia et al., 2004; Christophe et al., 2018).

However, samples contaminated by the post-depositional incorporation of intrusive (non-native) grains may have more complex distributions of D_e values. Estimating the D_e values of the native grains in such samples is especially challenging, because the dose distributions may contain distinct populations of grains superimposed on a broad dose continuum. In nature, post-depositional mixing of grains in unconsolidated sediments is ubiquitous at some scale, so consideration of sample context is critical. So, too, is a statistical model that can reliably extract the D_e associated with the population of native grains from the dose distribution.

Many of the most commonly used statistical models applied to D_e distributions were introduced to OSL dating following their earlier introduction in the context of fission-track dating (Galbraith and Green, 1990; Galbraith and Laslett, 1993; Galbraith, 2005; Galbraith et al., 1999; Galbraith and Roberts, 2012). Originating from the common dose model (CoDM), which computes the inverse-variance weighted mean based on the experimental error of each D_e value, extensions of this model have sought to better explain the observed overdispersion and asymmetry of empirical D_e distributions. The simplest extension is the central dose model (CDM), which adds a single (Gaussian) overdispersion term to the CoDM.

More sophisticated approaches have used both discrete and continuous mixtures of the CDM to model various physical processes thought to underpin the data-generating mechanism. Examples include the finite mixture model (FMM), which can be applied to single-grain distributions composed of multiple, discrete D_e components (Roberts et al., 2000; Sivia et al., 2004), the minimum dose model (MNDM), which is often applied to samples that had been partially bleached prior to burial (Galbraith et al., 1999; Arnold and Roberts, 2009), and the maximum dose model (MXDM). The latter has been used for samples that consist of fully bleached grains (the native grains of interest) with a proportion of younger, intrusive grains or grains that have been bleached after deposition (Olley et al., 2006; Galbraith and Roberts, 2012).

Within these classes of dose models (also often referred to as age models), further differentiation occurs depending on whether the modelled ‘central’ dose is computed from the expected value of the logged or unlogged D_e distribution (Arnold and Roberts, 2009; Galbraith and Roberts, 2012; Guérin et al., 2017), or whether maximum likelihood or Bayesian estimation methods are employed. The latter offers certain advantages in terms of statistical properties and the capacity to specify classes of discrete hierarchical models, such as the mixture distribution model (MD²; Christophe et al., 2018) and the Bayesian outlier model (BOM; Li et al., 2022). These models use discrete hierarchical distributions to (conditionally) assign mixture-component membership.

In this paper, we develop an asymmetric Laplacian (i.e., a two-sided exponential) mixture model (ALMM) that extends the standard CDM by adding two new parameters: one each to characterise the rate of both upward and downward (statistical) mixing processes; the CDM result is obtained if there is no mixing. We base the ALMM on the empirical observation that the relative abundance of zero-dose (i.e., fully bleached) grains in samples collected from the upper levels of the two Nawarla Gabarnmang data sets declines approximately exponentially

with depth. This post-depositional mixing pattern is consistent with the results of previous studies of deposits affected by pedoturbation (Bush and Feathers, 2003; Bateman et al., 2007; Wilkinson et al., 2009; Stockmann et al., 2013; Johnson et al., 2014; Gliganic et al., 2016).

We apply the ALMM to two data sets of vertically contiguous samples (16 samples in one sequence and 18 samples in the other) for which the D_e distribution patterns, extent of overdispersion, and initial CDM estimates suggest significant post-depositional mixing, thereby prohibiting reliable age estimation using the CDM. The ages estimated using the ALMM are validated by radiocarbon ages for charcoal fragments collected from sediments deposited within the reliable time range of the method, and are robust to additional measurement uncertainty. All analyses are undertaken in a Bayesian setting, but we provide an analytical evaluation of the model likelihood that can be used to estimate the ALMM parameters in a maximum likelihood setting.

We introduce the ALMM in the context of compound Gaussian distributions, which encompasses most of the commonly used dose models and allows similarities and differences between models to be viewed graphically by comparing schematics of the associated mixing distributions. Furthermore, we discuss future directions including potential extensions of the ALMM (and other dose models) to hierarchical models for data sets of samples from multiple depths (hereafter referred to as multi-depth hierarchical models), with a view to improve inferential properties, reduce data requirements, and interpolate age-depth trends guided by stratigraphic constraints.

Sediment samples and OSL data

Study site

Nawarla Gabarnmang is a large rock shelter (32 m \times 23 m in area) formed in quartzite sandstone on the Arnhem Land plateau in northern Australia (David et al., 2011, 2013, 2019). Excavations have been conducted at several locations inside the shelter as squares 50 \times 50 cm in area, exposing shallow deposits (< 1 m thick) with abundant cultural remains and charcoal pieces.

In Square E, a fallen slab of painted rock has been dated by radiocarbon to 26.5–27.7 ka cal BP and a further 18 radiocarbon ages have been obtained from individual pieces of charcoal, extending its cultural sequence to at least 43.1–49.3 ka cal BP (David et al., 2013). In this paper, calibrated radiocarbon age ranges are expressed at 95.4% probability, using OxCal 4.4 (Bronk Ramsey, 2009) and the SHCal20 data set (Hogg et al., 2020). Radiocarbon ages have also been obtained from other excavation squares in the shelter (Square A, $n = 25$: David et al. 2011; Squares F and ILM, $n = 38$ and 13, respectively: David et al. 2019), attesting

to human occupation of the site by at least 50 ka cal BP. In Square E, stone artefacts were found in every excavation unit down to bedrock (72 cm depth), whereas artefacts recovered from Square ILM extended below the deepest excavation unit dated by radiocarbon and were underlain by culturally sterile deposits resting on bedrock at 80 cm depth.

OSL sample collection and preparation

In 2012, sediment samples were collected for OSL dating from the stratigraphic sequences exposed in Squares E and ILM. In Squares E (east profile) and ILM (south profile), a vertical column of 55 and 65 contiguous samples, respectively (i.e., samples stacked consecutively, with no intervening gaps), were collected from just below the surface down to bedrock. Most of the samples were collected in depth increments of 1 cm, to limit the extent of time-averaging of the depositional ages of the grains in each sample. In addition, two OSL samples were collected in small-diameter tubes from the basal, culturally sterile deposits in the south face of Square ILM. Our aim was to establish a chronology for the entire cultural sequence in Squares E and ILM and the underlying culturally sterile deposits in Square ILM. In this study, we focus on the deepest artefact-bearing stratigraphic unit (SU) in each of these two squares, SU7 in Square E and SU4 in Square ILM (David et al., 2013, 2019), from which 18 and 16 OSL samples, respectively, have been measured and analysed.

Quartz grains of 180–212 μm in diameter were obtained from each of the sediment samples using routine preparation procedures, including treatment with HCl acid and H_2O_2 solutions, followed by dry sieving, density separation using solutions of sodium polytungstate, and etching in HF acid to remove the alpha-irradiated layer around the surface of each grain (Aitken, 1998). The etched grains were rinsed in HCl acid to remove any precipitated fluorides, sieved again, and then mounted on single-grain aluminium discs drilled with an array of 100 holes of 300 μm depth and diameter.

D_e measurement and single-grain D_e distributions

Single-grain OSL measurements and D_e determinations were made using the SAR procedure, experimental conditions, and equipment adopted previously for Australian quartz (e.g., Wood et al., 2016; Clarkson et al., 2017; Norman et al., 2022). Grains were stimulated using a focused green (532 nm) laser for 2 s at 125°C following a preheat of 260°C for 10 s in the natural and regenerative dose cycles and 160°C for 5 s in each test dose cycle. The first 0.22 s of OSL decay was used for D_e determination and the mean count recorded over the last 0.3 s was subtracted as background. Under these measurement conditions, dose recovery tests (Galbraith et al., 1999) yielded a recovered dose/given dose ratio consistent with unity (0.99 ± 0.01) and little overdispersion of the recovered doses (0.042 ± 0.006). Irradiations were made using $^{90}\text{Sr}/^{90}\text{Y}$ beta sources (calibrated using a range of laboratory reference standards) and spatial variations in dose rate to individual holes were taken into account for

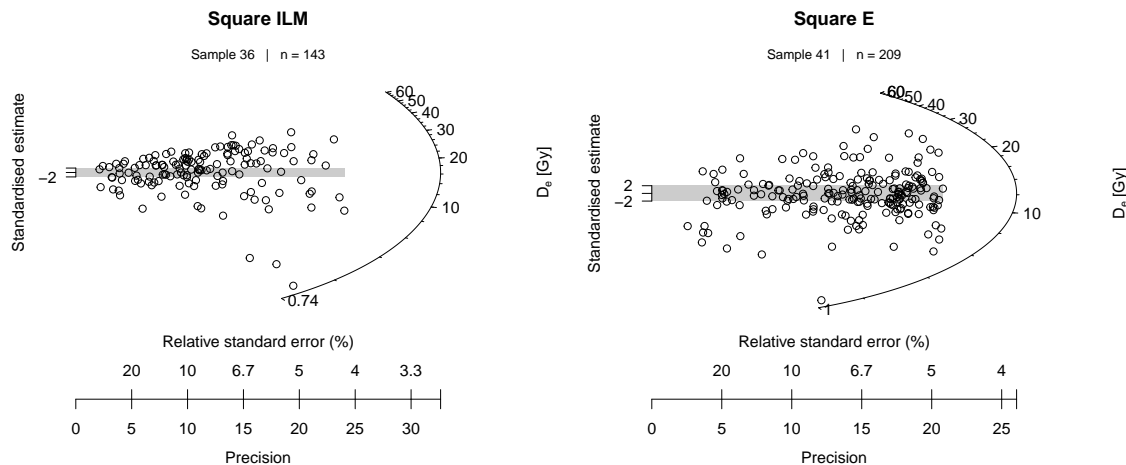


Figure 1: Radial plots of the D_e distributions for one sample from each of Squares ILM and E at Nawarla Gabarnmang. The grey bands are centred on the error-weighted mean D_e for each sample.

D_e determination.

For each sample, 500 grains were measured, and a dose-response curve constructed for each grain (including a zero regenerative dose to assess the extent of recuperation, and a duplicate regenerative dose to determine the recycling ratio). As a check on possible feldspar contamination, the OSL IR depletion ratio test (Duller, 2003) was also applied, using an infrared exposure of 40 s at 50°C at the end of the SAR sequence. OSL data were analysed using procedures published previously, including the rejection of aberrant grains using the quality-assurance criteria employed in other studies (e.g., Wood et al., 2016; Clarkson et al., 2017; Norman et al., 2022).

Of the grains measured for the Square E and Square ILM samples, 17–51% and 20–40% were accepted for D_e estimation, respectively. The OSL decay curves typically decline rapidly to instrumental background (consistent with the signal originating from the fast OSL component) and the D_e values rarely exceed 100 Gy, so they fall within the reliable dose range for quartz. Sample D_e values estimated using the CDM give OSL ages that increase with depth, but the D_e distributions are highly overdispersed (Figure 1), with σ_b values ranging from 0.50 ± 0.03 to 0.85 ± 0.05 for the Square E samples and from 0.55 ± 0.03 to 0.79 ± 0.05 for the Square ILM samples.

These overdispersion values are larger than expected for a population of well-bleached grains that have remained undisturbed and exposed to similar environmental dose rates since deposition (e.g., Arnold and Roberts, 2009, Table 4). If the overdispersion reflects the non-random vertical mixing of younger grains into older deposits after burial (e.g., due to sediment disturbance by human activity), then use of models that estimate the sample D_e based on the central dose of the distribution, such as the CDM and the average dose model (ADM: Guérin et al., 2017), are likely to underestimate the OSL ages of the native grains. Conversely, if

grains are moved upwards from stratigraphically deeper and older deposits, for example by termites or ants (Rink et al., 2013), then the OSL ages may be overestimated.

Environmental dose rates

The dose rates for the samples were estimated using the same methods, instruments and data-analysis procedures as those described by Clarkson et al. (2017). Beta dose rates were measured for each sample using a low-level beta counter and gamma dose rates were measured by *in situ* gamma spectrometry. Given the shallow depth of the deposits (72 cm in Square E and 80 cm in Square ILM), the penetration distance of gamma rays through sediment (~ 30 cm), and the low variability in gamma dose rates down-profile, we estimated the gamma dose rates from 3 measured locations in each sample column in Squares E and ILM (11–19 cm vertical spacing between locations). We assumed an internal dose rate of 0.03 ± 0.01 Gy/ka for all samples and estimated the cosmic-ray dose rates using published equations (Prescott and Hutton, 1994), making allowance for site altitude, geomagnetic latitude, density and thickness of rock and sediment overburden, and the angular distribution of cosmic rays.

The total dose rates for samples from Square E (SU7) and Square ILM (SU4) range from 0.55 ± 0.02 to 0.63 ± 0.02 Gy/ka and from 0.65 ± 0.03 to 0.81 ± 0.03 Gy/ka, respectively. The deposits in both squares consist mainly of compact and consolidated dry brown quartz sand and silt derived from the surrounding landscape and from weathering of the sandstone in which the rock shelter is formed (David et al., 2013, 2019). Ash and charcoal from anthropogenic fires are more abundant higher up the stratigraphic sequences (e.g., SU1 and SU2 in Square ILM).

Post-depositional mixing

Squares E and ILM are located close to the edge of the rock shelter, so the quartz grains were almost certainly exposed to sufficient sunlight to empty the OSL traps at the time of deposition. The D_e distributions are also unlike those obtained for samples that have been partially bleached prior to burial—a cluster of values in the low-dose region of the distribution, with a large spread of higher D_e values (e.g., Jankowski et al., 2016). Furthermore, given the homogeneous, quartz-dominated composition of the deposits in both excavation squares, grain-to-grain variations in beta dose rate are unlikely to be the principal cause of the highly overdispersed D_e distributions (Fu et al., 2022).

The latter might, instead, be due to post-depositional mixing. The lack of multiple, discrete D_e components in the single-grain distributions suggests that any such mixing did not take place as distinct temporal events. We hypothesised, therefore, that each sample contains a proportion of intrusive grains embedded within the population of native grains and examined the D_e distributions for the presence of ‘modern’ grains (i.e., those with D_e values consistent

with zero) to estimate the shape of the penetration profile for the intrusive grains. Assuming the same general pattern of vertical mixing has occurred throughout the history of sediment deposition at this site, but allowing the rate of penetration to vary, the D_e estimates for the native grains in each sample can be reconstructed using the ALMM, as we describe in the following sections.

Theory

A class of compound Gaussian dose models

The context for statistical dose modelling in the present study is the availability of an OSL data set comprising a sample of D_e measurements D_i , $i = 1, \dots, N$ and corresponding estimates of the measurement errors $\sigma_{D,i}$.

Dose models are often specified on the log scale, expressed as a probability density of the pointwise log-dose $d_i = \log D_i$, with associated measurement error $\text{se}(d_i)$, approximated as $\sigma_{d,i} = \sigma_{D,i}/D_i$. For Gaussian-based models, the log scale is generally preferred for non-modern samples due to the (almost) strictly positive values of the measured D_e values and the tendency of the measurement errors to increase in proportion to the mean (Galbraith and Roberts, 2012). For young and modern samples, statistical models of the unlogged doses are sometimes used (Arnold and Roberts, 2009). The modelling approaches presented in this paper can be adapted for use with unlogged data, although we use logged data as the default scenario.

A statistical log-dose model is characterised by a pointwise probability density $p(d_i | \theta, \sigma_{d,i})$, conditional on measurement error $\sigma_{d,i}$ and a vector of distributional parameters θ . For a given log-dose distribution, the corresponding distribution of the unlogged dose D_i is

$$p(D_i | \theta, \sigma_{D,i}) = \frac{1}{D_i} p(\log D_i | \theta, \frac{\sigma_{D,i}}{D_i}), \quad (1)$$

where $\frac{1}{D_i} = \frac{d}{dD_i} \log D_i$ effects the change of variable. As a base model for further development, we recall the pointwise probability density of the CDM

$$p_{\text{CDM}}(d_i | d_0, \sigma_0, \sigma_{d,i}) = (2\pi\sigma_i^2)^{-1/2} \exp\left(\frac{(d_i - d_0)^2}{-2\sigma_i^2}\right), \quad (2)$$

where d_0 is the central log-dose, σ_0 is the overdispersion (equivalent to σ_b in Galbraith et al. 2005), and $\sigma_i^2 = \sigma_0^2 + \sigma_{d,i}^2$. A broad class of probability distributions can be obtained from the CDM by compounding the Gaussian distribution (2) with a mixing distribution (or

mixing function) ω , expressed as

$$p(d_i | d_0, \sigma_0, \theta, \sigma_{d,i}) = \int \omega(d, \sigma | d_0, \sigma_0, \theta) p_{\text{CDM}}(d_i | d, \sigma, \sigma_{d,i}) dd d\sigma, \quad (3)$$

where the integration of p_{CDM} against ω generates a CDM-Gaussian mixture that can be either discrete, continuous, or both, depending on the functional form of ω . The mixing distribution is a probability density function satisfying $\int \omega dd d\sigma = 1$. In the simplest case, where ω is a Dirac delta function $\delta(x, y) \equiv \delta(d - x) \cdot \delta(\sigma - y)$ (see Appendix A.2 for details), the distribution $p(d_i | d_0, \sigma_0, \sigma_{d,i}, \theta)$ contains a single Gaussian component: $p_{\text{CDM}}(d_i | x, y, \sigma_{d,i})$. Thus, the CDM and its submodel, the CoDM, can be recovered from (3) by setting ω to $\delta(d_0, \sigma_0)$ and $\delta(d_0, 0)$, respectively.

The class of compound distribution models (3) provides a unifying framework to express many of the most commonly used dose models. Several of these models are summarised in Table 1 where, for each model, a mathematical expression of the associated mixing function is accompanied by a visual schematic of the mixture components, as well as representative plots of the corresponding pointwise probability density functions. The final row of the table expresses the new ALMM, which we derive in the following section along with our reasons for adopting this approach.

The ALMM

Exponential mixing distributions

To account for both upward and downward vertical mixing processes, we introduce an asymmetric Laplacian (or two-sided exponential) mixing distribution defined as follows:

$$\omega(d | d_0, \tau, \eta) = \begin{cases} \frac{1}{\tau + \eta} \exp(\frac{1}{\tau}(d - d_0)) & d < d_0 \\ \frac{1}{\tau + \eta} \exp(\frac{1}{\eta}(d_0 - d)) & d_0 < d. \end{cases} \quad (4)$$

The mixing distribution has maximum density at the central log-dose d_0 , decaying either side at a rate determined by τ and η , which parameterise downward and upward mixing processes, respectively. The asymmetry of the distribution allows for different rates of mixing in the upward and downward directions, with empirical studies supporting the intuitive notion that downward mixing rates should be greater than upward rates (Wilkinson et al., 2009), although upwards rates may not be negligible (Heimsath et al., 2002; Rink et al., 2013). For this reason, a two-sided exponential is preferred over a one-sided distribution.

Since the mixture is defined on the (log) dose scale, rather than a spatial coordinate, the two rate parameters account implicitly for changes in vertical-mixing-, deposition- and dose-rates as a function of depth (see Appendix A.1 for supporting analyses). Although the confounding of these different rate types in the definition of τ and η prohibits their direct interpretation


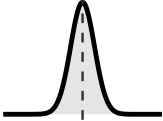
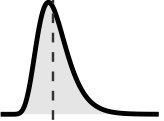

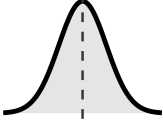
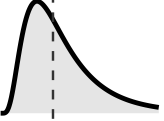
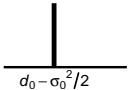
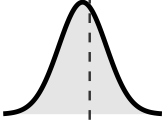
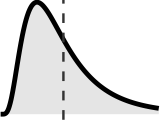
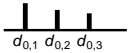
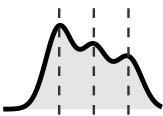
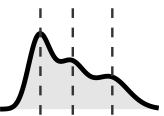
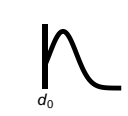
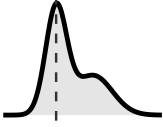
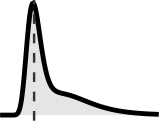
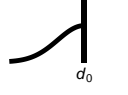
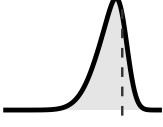
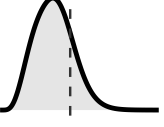

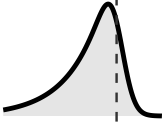
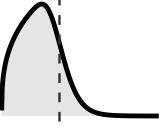
Model name	$\omega(d, \sigma d_0, \sigma_0, \theta)$	ω -plot	$p(d d_0, \sigma_0, \theta)$	$p(D D_0, \sigma_0, \theta)$
Common dose model (CoDM)	$\delta(d_0, 0)$			
Central dose model (CDM)	$\delta(d_0, \sigma_0)$			
Average dose model (ADM)	$\delta(d_0 - \sigma_0^2/2, \sigma_0)$			
Finite mixture model (FMM)	$\sum_{k=1}^K w_k \delta(d_0, k, \sigma_0, k)$			
Minimum dose model (MNDM-4)	$q \delta(d_0, \sigma_0) + \delta(\sigma_0)(1 - q)N_t^+(d d_0, \sigma_t, \gamma_t)$			
Maximum dose model (MXDM-3)	$q \delta(d_0, \sigma_0) + \delta(\sigma_0)(1 - q)N_t^-(d d_0, \sigma_t)$			
Asymmetric Laplacian mixture model (ALMM)	$\begin{cases} \frac{\delta(\sigma_0)}{\tau + \eta} \exp(\frac{1}{\tau}(d - d_0)) & (d < d_0) \\ \frac{\delta(\sigma_0)}{\tau + \eta} \exp(\frac{1}{\eta}(d_0 - d)) & (d_0 < d) \end{cases}$			

Table 1: Commonly used dose models and the ALMM expressed as compound Gaussian distributions. The mixing distributions ω are plotted schematically in the third column with the Dirac delta function $\delta(x, y)$ represented as a vertical line at $d = x$. Representative plots of the pointwise (compound) probability density functions for the log-dose d_i and unlogged-dose $D_i = e^{d_i}$ are shown in the final two columns, where the dashed vertical lines depict the ‘central’ log-doses d_0 and unlogged-doses $D_0 = e^{d_0}$, respectively. The suffixes ‘-3’ and ‘-4’ denote the three- and four-parameter versions of the stated models, respectively.

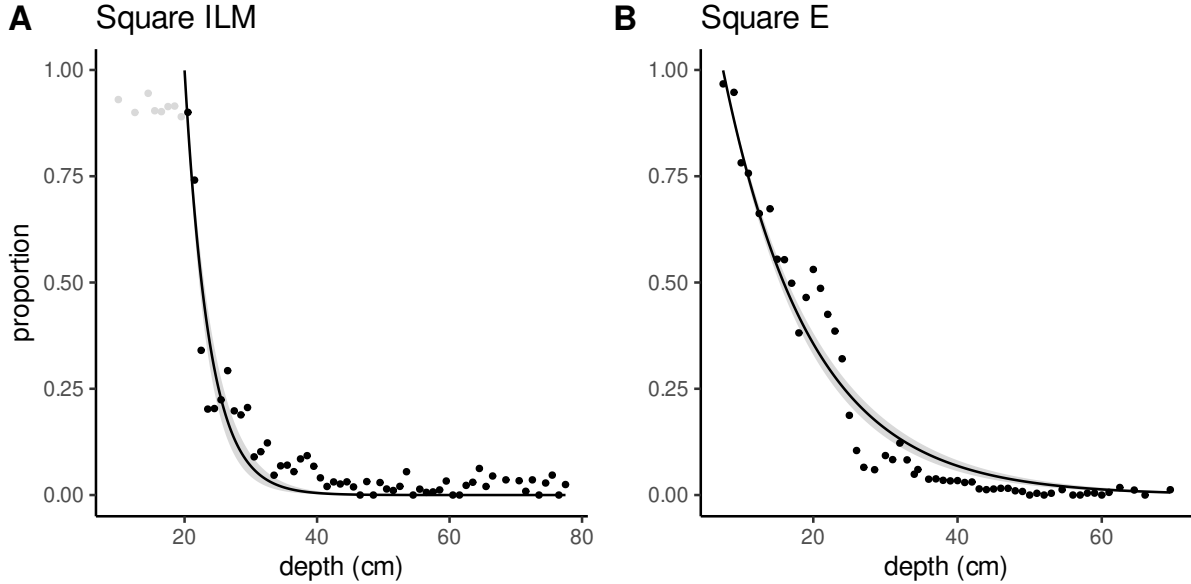


Figure 2: Proportion of zero-dose grains as a function of depth for Squares ILM and E at Nawarla Gabarnmang. Grains are defined as zero-dose if their equivalent dose values are consistent with 0 at 2 standard errors. Trend lines are of the form $y = \exp(-\lambda \times \text{depth})$, estimated with additive residual errors. The λ estimates and 95% credible intervals are 0.271 (0.235, 0.314) and 0.083 (0.077, 0.089) for Squares ILM and E, respectively. Samples located less than 20 cm from the surface in Square ILM (light grey points) were omitted from trend fitting due to their zero-dose proportions being relatively constant close to 1

as physical mixing rates (i.e., rates expressed in terms of mass per unit area per unit time), their inclusion in the model permits the parameter d_0 to be interpreted as the central dose of the original (i.e., unmixed or native) grain population.

The use of an exponential mixing distribution, as opposed to a half-Gaussian or other type of decay model, is motivated by empirical studies of bioturbation, including analyses of the intrusion rates of tracers from the soil surface. [Wilkinson et al. \(2009, Figure 5\)](#) studied biotic activity through the soil profile, finding exponential trends for several bioturbation indices as a function of depth. [Johnson et al. \(2014\)](#) modelled bioturbation as a depth-dependent diffusion process and showed that an exponential diffusion coefficient fitted their data better than a linear alternative. [Bateman et al. \(2007, Figures 2 and 3\)](#) and [Gliganic et al. \(2016, Figure 7a\)](#) found that the proportion of zero-dose grains (i.e., grains with D_e values consistent with recent bleaching, thereby representing grains that have been recently mixed downward from the surface) declined exponentially with depth in the top 60–80 cm of sand mantles; and [Bush and Feathers \(2003\)](#) similarly noted a rapid decrease in the concentration of zero-dose grains with depth in the top 35 cm of anthropogenic earthen mounds.

We analysed the proportion of zero-dose grains for the two Nawarla Gabarnmang data sets, finding clear evidence of exponentially decaying intrusion rates for downward-moving grains, with a steep rate of decay in the upper ~ 30 cm (Figure 2).

Of course, the exponential mixing of grains in the (vertical) spatial coordinate will only correspond to exponential mixing on the (log) dose scale if the underlying trend of (log) dose with depth can be approximated as locally linear. In practice, it may be difficult to determine the validity of this approximation, given the goal of statistical dose modelling is typically to estimate the central dose of depth-specific samples; the problem is further complicated by any depth-dependence of the dose rates. Despite these uncertainties, some of which could potentially be addressed using multi-depth hierarchical approaches (see *Discussion*), modelling the grain mixture on the (log) dose scale is consistent with existing approaches such as the FMM, MXDM/MNDM, and the (discrete) mixture distribution model (MD², Christophe et al., 2018).

As with all applications of statistical modelling, model-validation techniques (e.g., posterior predictive checks or independent reference values) and formal model-selection methods (e.g., cross validation or information criteria) play an important role in assessing the merits of candidate models and the validity of inferred quantities (Gelman et al., 2013; Gabry et al., 2019; Yates et al., 2022).

Model likelihood

To derive the ALMM likelihood, we substitute (4) into (3), making the simplifying assumption that all mixture components share a common overdispersion value $\sigma = \sigma_0$, to yield the following four-parameter probability density and its analytical evaluation derived using standard methods of integral calculus:

$$\begin{aligned}
 p_{\text{ALMM}}(d_i | d_0, \sigma_0, \tau, \eta, \sigma_{d,i}) &= \int_{-\infty}^{\infty} \omega(d | d_0, \tau, \eta) p_{\text{CDM}}(d_i | d, \sigma_0, \sigma_{d,i}) dd & (5) \\
 &= \frac{1}{2(\tau + \eta)} \exp\left(\frac{1}{2\tau} \left(2x_i + \frac{\sigma_i^2}{\tau} - 2d_0\right)\right) \operatorname{erfc}\left(\frac{-d_0 + x + \frac{\sigma_i^2}{\tau}}{\sqrt{2}\sigma_i}\right) + \\
 &\quad \frac{1}{2(\tau + \eta)} \exp\left(\frac{1}{2\eta} \left(-2x_i + \frac{\sigma_i^2}{\eta} + 2d_0\right)\right) \operatorname{erfc}\left(\frac{d_0 - x + \frac{\sigma_i^2}{\eta}}{\sqrt{2}\sigma_i}\right), & (6)
 \end{aligned}$$

where $\operatorname{erfc}(x) = 2\pi^{-1/2} \int_x^{\infty} e^{-t^2} dt$ is the complementary error function: a one-parameter special function directly related to the standard normal cumulative density function. Evaluating the likelihood using the form (6) significantly reduces computation time compared to numerical integration of (5) due to the rapid computation of $\operatorname{erfc}(x)$. Given data, the model parameters can be estimated using maximum likelihood (solved numerically) or using Bayesian methods with appropriate specification of priors. In the following section, we apply the ALMM to the data sets for Square ILM (SU4, n = 16 samples) and Square E (SU7, n = 18 samples) using a Bayesian approach, and use the available radiocarbon chronology to validate the estimated OSL ages for the native grains in each sample.

Although the CDM and MXDM are almost certainly inappropriate for use with these particular data (due to their large overdispersion values), we perform a sensitivity analysis of the posterior age distributions for the ALMM, CDM and MXDM across a range of fixed overdispersion values applied to a representative sample. This analysis investigates the sensitivity of the inferred age distributions to overdispersion estimates and/or changes in overall measurement uncertainty, providing general insights into the effect of different mixing assumptions on the estimated ages.

Parameter estimation

The ALMM was fitted to each of the samples using the new R package `rstanos1` (Aandahl and Yates, 2023) that implements full Bayesian inference via `rstan`, an R language interface for the Stan statistical modelling platform (Stan Development Team, 2022). The implementation uses Hamiltonian Monte Carlo methods in combination with no-u-turn sampling (NUTS, Hoffman and Gelman, 2014) for efficient posterior estimation. For all parameters, we used the robust and weakly-informative prior distribution $\text{Cauchy}(0, 1)$. For each model, we ran four chains of 2000 iterations (including 1000 warm-up iterations) and chain convergence was established using the improved \hat{R} statistic (Vehtari et al., 2021) together with visual inspection of the chains.

For each OSL sample, the age distribution of the native grains is derived from the posterior log-dose distribution using

$$A_s = D_s/B \quad (7)$$

where $D_s = e^{d_s}$, B is the mean estimated dose rate for the OSL sample, and s indexes the posterior samples. For simplicity, we simply divide the posterior samples of the central dose by the mean dose rate, although it would be straightforward to use the estimated standard error of the dose rate to propagate the dose-rate uncertainty using, for example, delta-method approximations or simulation of the dose-rate distribution (see also Mercier et al. (2022) and Fu et al. (2022) for recent perspectives).

Age inference

The ALMM-estimated age distributions (7) of the native grains in both data sets are shown in Figure 3. The sample closest to the top of SU4 in Square ILM has a substantially lower age (mean = 15.2 ka) than the other samples from this square, most likely due to grain-mixing across the interface with the overlying SU (i.e., SU3). The second-to-top sample has a wide distribution, bridging the transition to the older samples that comprise the remainder of SU4. The latter follow an overall trend of increasing age with depth. The 11 radiocarbon ages for SU4 validate the ALMM age estimates. The ages for the uppermost seven samples

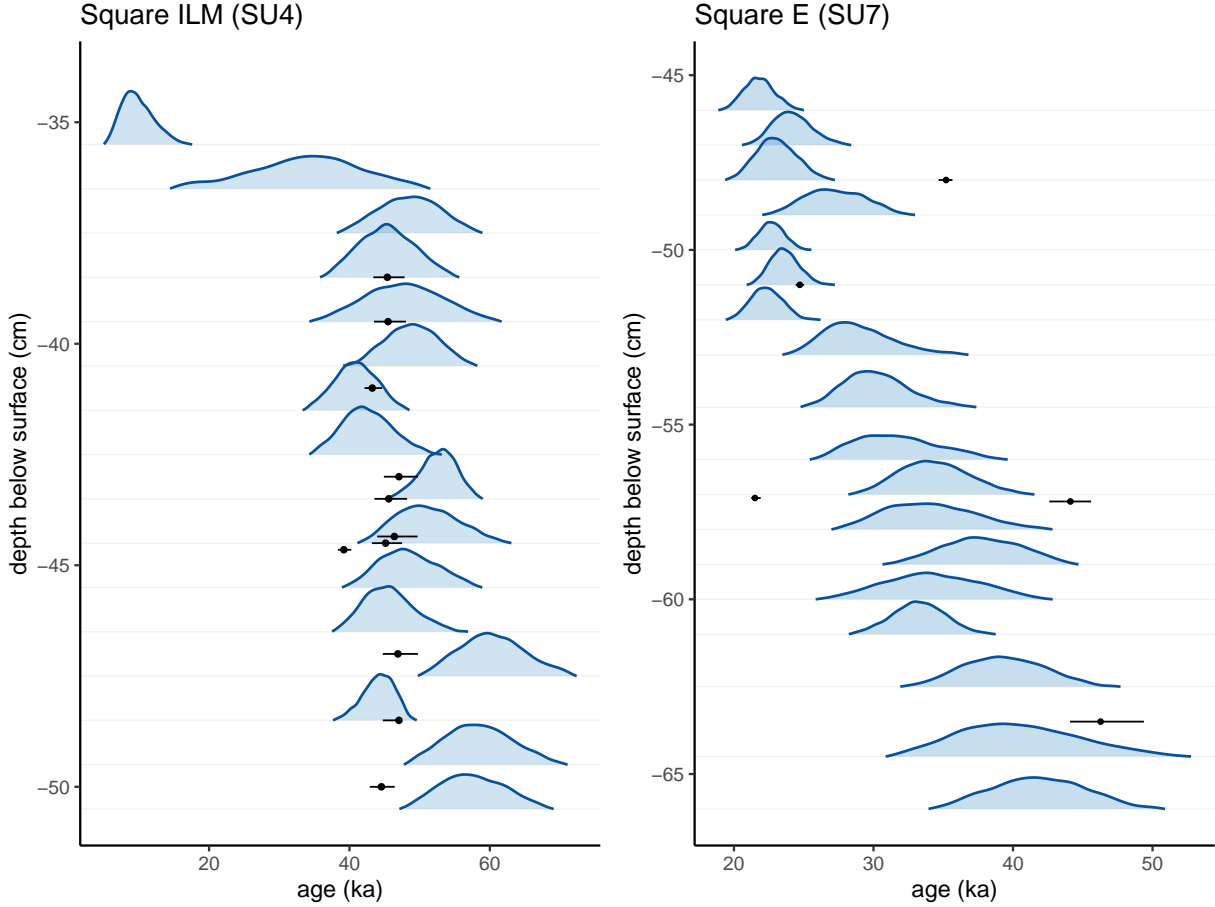


Figure 3: Posterior OSL age distributions and radiocarbon determinations for Squares ILM and E. The blue curves denote kernel density estimates for the posterior distribution of the ALMM-estimated central ages of the native grains in each sample. The black points and horizontal lines are the posterior medians and 95.4% credible intervals for calibrated radiocarbon ages of charcoal fragments from Squares ILM (David et al., 2019, Table 1) and E (David et al., 2013, Table 1).

in Square E (SU7) show no obvious trend with depth, but then increase steadily below a depth of ~ 52 cm. Only five radiocarbon age estimates are available for comparison and two of these differ by more than 20 ka, despite being sampled at approximately the same depth, rendering it difficult to externally validate the ALMM age distributions for this square.

The posterior estimates of the mixing and overdispersion parameters are shown in Figure 4. For both data sets, the downward mixing rate τ (shown in dark blue) is consistently estimated to be larger than upward rate η (shown in light blue). The median overdispersion values (shown in black) are mostly less than 0.25; a few exceed 0.4, which suggests model misspecification (i.e., failure to adequately represent the data-generating process) for these samples. As a function of depth, all three parameters display general trends (e.g., downward mixing rates generally decrease with depth, whereas upward mixing rates and overdispersion values exhibit no such pattern) suggesting the possible merits of hierarchical regression,

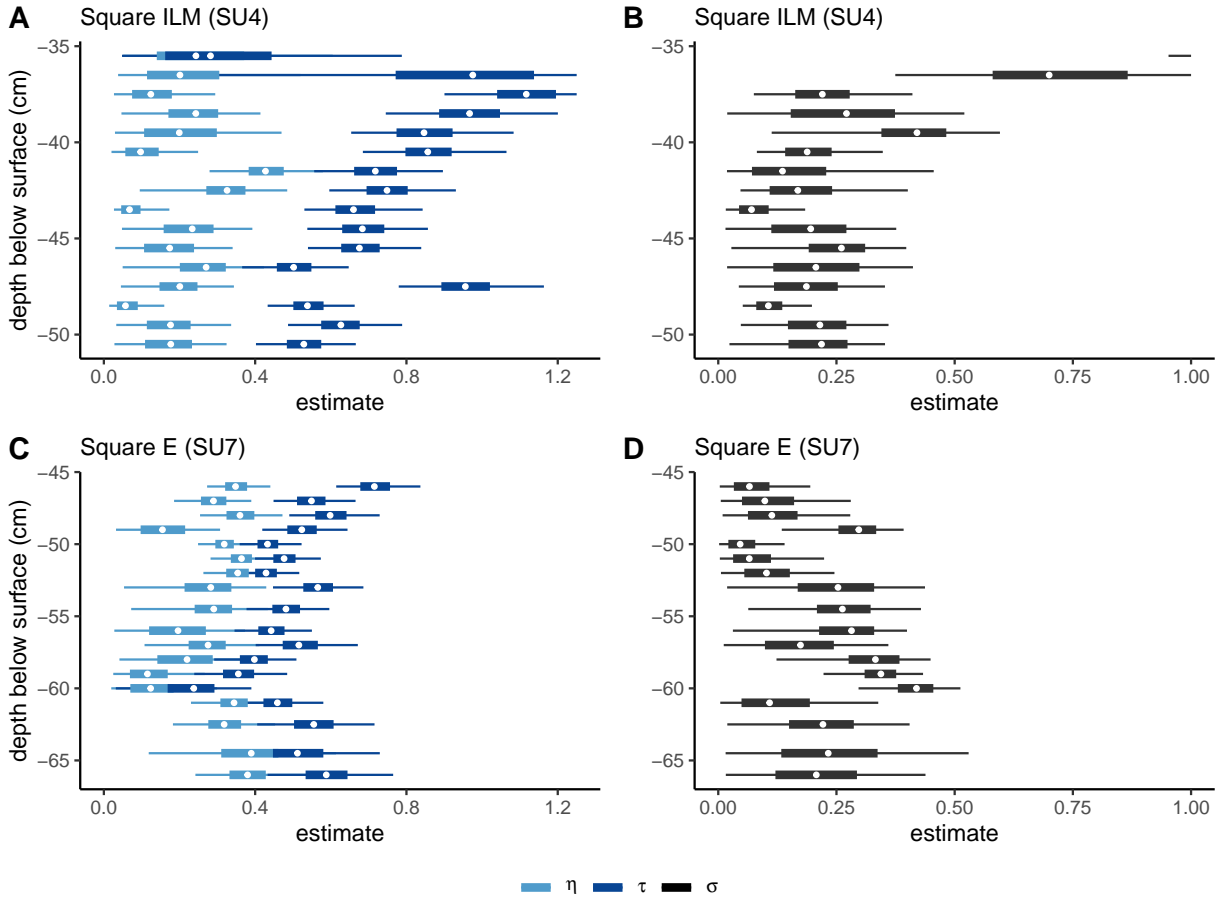


Figure 4: Posterior estimates of the mixing and overdispersion parameters for Squares ILM and E. The thin and thick lines display the 95% and 50% credible intervals, respectively, and the white circles are the posterior medians. The two mixing parameters are plotted together (left panels) and the overdispersion parameter is shown separately (right panels). The large outlying overdispersion value for the topmost sample in Square ILM is omitted from panel B.

whereby sample-specific estimates are regularised towards a global trendline (see *Discussion* for elaboration).

Sensitivity to the overdispersion parameter

In OSL dating, the distribution of $(\log) D_e$ values about the central $(\log) D_e$ is commonly overdispersed relative to the measurement errors of the individual grains or multi-grain aliquots (e.g., Galbraith et al., 2005; Arnold and Roberts, 2009). Typical values of the overdispersion parameter σ_0 for single grains of quartz from well-bleached samples range from 0.1 to 0.3 (Arnold and Roberts, 2009, Table 4). The CDM estimates σ_0 from the spread in data, whereas it is common to supply a fixed value of σ_0 when implementing

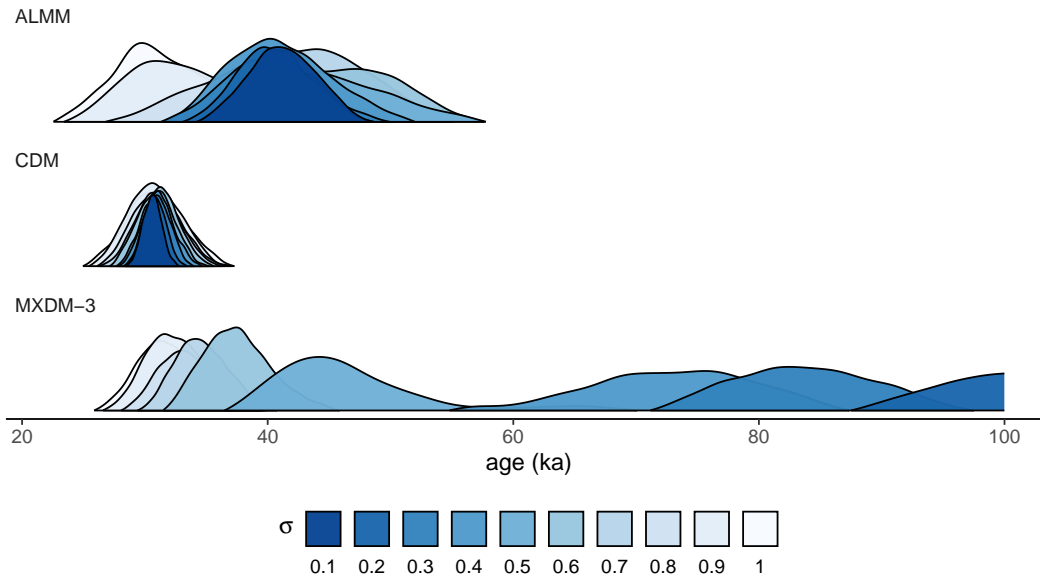


Figure 5: Sensitivity of posterior age distributions to changes in the fixed value of σ for a selected sample (Square ILM, sample depth = 41.5 cm). For ease of comparison, the MXDM distribution for $\sigma_0 = 0.2$ is truncated on the right and the distribution for $\sigma_0 = 0.1$ (mean age = 137 ka) is omitted altogether.

other models (e.g., MXDM, MNDM and FMM). The supplied value can be determined independently (e.g., by applying CDM to a fully bleached or unmixed sample analogue) and it may comprise an intrinsic component due to aspects of the shared measurement process (Galbraith et al., 2005; Galbraith and Roberts, 2012; Guérin et al., 2017); the latter can be estimated from dose recovery experiments. Often, however, an arbitrary value or set of values for σ_0 is chosen from within the typical range. In the absence of prior information, it is preferable to estimate σ_0 because inferred ages have been shown to be sensitive to the choice of σ_0 in simulations (Peng et al., 2020). Large estimated values (e.g., $\sigma_0 > 0.4$) may indicate model misspecification or the influence of some other source of dispersion that is not factored into dose recovery tests, such as beta dose heterogeneity (Fu et al., 2022).

Here we take a single representative sample from Square ILM and perform a sensitivity analysis by comparing the posterior age distributions for the ALMM, CDM and three-parameter MXDM across a range of fixed overdispersion values: $\sigma_0 = 0.1, 0.2, \dots, 0.9, 1$. We extend well beyond the typical range to include the (large) estimated values of σ_0 for the CDM and MXDM. Our aim is to investigate the sensitivity of age estimates as a function of the chosen mixing distributions and their subsequent capacity to explain variation in the data. All models are fitted using the R package `rstanos1`.

The age distributions for each model for all 10 of the fixed σ_0 values are shown in Figure 5. The CDM is the least sensitive to changing values, but underestimates the central age in the presence of mixing that is predominantly downward. The MXDM is highly sensitive and clearly overestimates the age for $\sigma_0 \leq 0.4$, whereas the ALMM is relatively insensitive

for low σ_0 values. When estimating (rather than fixing) the overdispersion value for this sample, the expected posterior σ_0 estimates are 0.14, 0.72 and 0.67, for the ALMM, CDM and MXDM, respectively. For the latter two models, these large values indicate failure to adequately explain variation in the data, thus invalidating subsequent age inferences due to misspecification bias (here a substantial downward bias).

The sensitivity analysis shows that ALMM age inference is robust to changes in the value of the overdispersion parameter (the estimated expected value is less than 0.4). Further, the analysis shows that it is not sufficient to simply fix σ_0 to a value deemed acceptably low for use with the MXDM, since such a value is far from the posterior mean of the estimated σ_0 (here 0.67) and the corresponding age estimate is significantly overestimated as a result. Despite its low sensitivity, the CDM is obviously an inappropriate model for vertically mixed samples such as these, as are other models used to estimate ages based on the central dose, such as the ADM. The relative sensitivities of these models to σ_0 for this particular sample are representative of the general trends across the two data sets.

Discussion

Summary

We have introduced a new dose model for application to vertically mixed OSL samples. The model accounts for mixing processes in both the upward and downward directions, estimating the central dose and associated overdispersion of the native (i.e., unmixed) grain population. The ALMM extends the family of existing dose models, here unified under the umbrella of compound Gaussian distributions (or CDM mixtures). Within this statistical framework, each model is characterised by a mixing distribution that can be plotted schematically to provide an intuitive visual summary of the mixture components.

We applied the ALMM to two highly mixed data sets. One of these has a sufficient number of (independent) radiocarbon age estimates to provide a strong validation of the model's predictive performance. Moreover, we performed a sensitivity analysis that demonstrated the robustness of the ALMM age estimates to changes in the modelled overdispersion, or, equivalently, to additional measurement uncertainty. The same analysis compared age estimates for the ALMM, CDM and MXDM, which suggested that the CDM and MXDM will respectively under- and over-estimate the ages of the native grains in such data sets, for typical values of the overdispersion parameter.

As a CDM mixture, the ALMM reduces to the ordinary CDM in the limit of zero mixing rates (i.e., $\tau \rightarrow 0, \eta \rightarrow 0$), making the model appropriate for OSL samples across a range of mixing scenarios. Computationally, it can be difficult to fit the ALMM as mixing parameters approach the CDM limit (e.g., Monte Carlo chains are slow to converge); in this case, we recommend fitting the CDM directly.

Choice of mixing distribution

In the context of post-depositional mixing, the validity of age inference via statistical dose mixture modelling depends on the selection of an appropriate mixing distribution. To reflect the underpinning physical processes (e.g., bioturbation and diffusion), the mixing distribution must be asymmetric (to accommodate differing rates of mixing in each direction) and decay either side of the central dose (as displacement probabilities decrease with vertical distance from the depositional level of the sample), yet there remain many available choices beyond the Laplacian model we have introduced. On the basis of empirical studies, we have argued for an exponentially shaped mixture, but the translation of these spatial mixing trends to a corresponding distribution on the log-dose scale is difficult to validate. Possible ways forward include the use of non-parametric mixtures (e.g., [Christophe et al., 2018](#)), with prior distributions used to impose shape constraints, or to hypothesise a set of candidate mixing functions (e.g., skew-normal, two-sided half Cauchy, etc.) and use formal model-selection techniques to choose among them ([Yates et al., 2022](#)). This latter approach could be particularly useful when applied in a hierarchical context (see *Future work*), where the ‘borrowing of strength’ across multiple samples would maximise use of the available information to compare model performance. For Bayesian models fitted using Monte Carlo sampling, approximate leave-one-out cross validation is a robust and theoretically rigorous approach to model comparison based on information-theoretic principles and is easily implemented using the R package `loo` ([Vehtari et al., 2017](#)).

Marginal versus conditional approaches

The uptake of Bayesian methods in dose modelling has generated new possibilities for the implementation of mixture models, yet care must be taken to distinguish between marginal (i.e., integrated) likelihood models and their conditional analogues—ALMM is an example of the former. To illustrate the two approaches, we recall the structure of the MNDM, which nominally comprises two discrete components: fully-bleached grains and partially-bleached grains. Both components are CDMs, but the central dose of the latter component is itself drawn from a truncated normal distribution. Using a marginal approach, the pointwise probability density is obtained by first integrating over the truncated distribution and then taking a weighted average of the discrete components. Using a conditional approach, however, the MNDM probability distribution is a single CDM conditional on both the pointwise discrete-component membership z_i (e.g., $z_i = 0$ [fully-bleached] or $z_i = 1$ [partially-bleached]) and, if $z_i = 1$, on a pointwise central dose estimate $d = d_{0,i}$; otherwise $d = d_0$. The original MNDM was specified as a marginal model ([Galbraith et al., 1999](#)), whereas recent publications have emphasised a conditional perspective ([Christophe et al., 2018](#); [Li et al., 2022](#)).

The conditional model requires discrete sampling of $z_i \sim \text{Bernoulli}(p)$ (i.e., Bayesian methods must be used) and has substantially more parameters than the marginal model. Indeed, the low ratio of data points to model parameters in the latter formulation means that prior knowledge is likely to be heavily influential. In Monte Carlo approaches to Bayesian estimation, the conditional approach is straightforward to implement, requiring only sampling from, rather than integration over, the mixing distribution. However, the marginal approach, which does require integration (analytical or numerical), is arguably more appropriate for

grain mixtures that result from continuous mixing processes, such as bioturbation. The latter marginalises over the uncertainty of the mixture distribution, thereby reducing model complexity, reducing fitting time and improving inferential properties (Gelman et al., 2013; Merkle et al., 2019; Yackulic et al., 2020). We have introduced the ALMM as a marginal mixture model (see (6)), for which individual grains are not assigned component membership (e.g., to a discrete, uncontaminated depositional level or population of origin), but are viewed as being drawn from a continuous mixture (or compound distribution).

Future work: hierarchical extensions

For clarity of exposition, we have introduced the ALMM as a single-depth model (i.e., the posterior age distributions were estimated individually for each sample), but it is a natural candidate for implementation using multi-depth hierarchical approaches. Drawing each depth-specific mixing parameter from a corresponding (prior) distribution has the potential to leverage information about mixing processes between depths, reducing the amount of data required at a single sampling depth and improving inferential properties due to statistical regularisation (Gelman et al., 2013). For example, a multi-depth ALMM likelihood can be written as

$$p_{\text{ALMM}}(d_{ij} | d_{0,j}, \sigma_{0,j}, \tau_j, \eta_j, \sigma_{d,ij}), \quad (8)$$

where d_{ij} denotes observation i within sample j . For the mixing and overdispersion parameters, it is reasonable to expect that samples which are physically closer will have estimates that are more similar due to their physically connected depositional and mixing histories. Examples of prior distributions for these positive-valued depth-specific parameters are

$$\begin{aligned} \log \tau_j &\sim N(\alpha_\tau + \beta_\tau x_j, s_\tau) \\ \log \eta_j &\sim N(\alpha_\eta + \beta_\eta x_j, s_\eta) \\ \log \sigma_{0,j} &\sim N(\alpha_\sigma + \beta_\sigma x_j, s_\sigma), \end{aligned} \quad (9)$$

where x_j is the depth of sample j ; that is, the distributional means of the log-transformed parameters are linear functions of depth for which the hyperparameters s_τ , s_η , and s_σ determine the degree of shrinkage towards the modelled means. For the central log dose $d_{0,j}$, a candidate prior is

$$d_{0,j} \sim N(a(x_j) + b_j, s_d), \quad (10)$$

where $b_j = \log B_j$ (the log of the dose rate in sample j) and $a(x)$ is the mean log age as a function of depth (cf. (A.13)). The log-age-to-depth trend can be flexibly modelled using non-parametric approaches such as smoothing splines (Wood, 2003), for which the interpolated age-to-depth trend through the sampled profile is

$$A(x) = e^{a(x)}. \quad (11)$$

The above is only one example of a candidate hierarchical structure. Non-linear age-to-depth trends can be formulated within the multi-depth context in a variety of ways, depending on the application of stratigraphic constraints (e.g., strictly increasing age-to-depth trends) and the propagation of age uncertainty into interpolated regions (e.g., using autocovariance functions to model increasing predictive uncertainty with distance from a sampled location (Blaauw and Christen, 2011)). Formal model-comparison approaches such as cross validation or information criteria, applied in conjunction with parsimonious selection principles, can be used to select among alternative structures on the basis of predictive performance, while mitigating concern for overfitting (Yates et al., 2021).

In principle, hierarchical structures can be used to elevate any single-depth model to a multi-depth analogue. In the multi-depth setting, individual distributional parameters can be pooled (i.e., common to all depths), unpooled (i.e., independent for all depths), or partially-pooled (i.e., drawn from a common distribution). Pooled estimates are the most parsimonious of these formulations, while unpooled estimates are equivalent to separate sample-by-sample estimation of parameters, as we have applied in this paper. Partially-pooled models are a particularly interesting avenue for future work because the appropriate use of prior distributions allows the data to determine the degree to which information is shared between samples. When data are scarce, partial pooling may allow the inference of age-depth trends where the paucity of data prohibits the fitting of independent single-depth models.

A further advantage of jointly estimating the age-depth trend and associated depth-specific mixing parameters is the elicitation of an explicit link between physical rates of sediment deposition and mixing on the spatial scale and statistical mixing rates on the (log) dose scale. For example, exponential decay in the sediment mixing rates on the spatial coordinate could be transformed into a corresponding decay function on the log dose scale to account for the modelled deposition rate and associated dose rates.

Conclusions

In this study, we introduced an asymmetric Laplacian mixture model (ALMM) for application to continuous mixtures in which individual grains have been displaced vertically in an upward or downward direction. The ALMM provides an estimate of the central dose of the ‘native’ grains present in a sample (defined here as grains in primary depositional context), assuming an exponential mixing distribution with depth, as has been observed in many real-life settings. We tested the model on two single-grain OSL data sets from an archaeological site in northern Australia and show that the resultant age estimates for the native grains are consistent with the available radiocarbon chronologies and are robust to changes in the modelled overdispersion value or additional uncertainty in OSL measurements. We estimated the model parameters using Bayesian methods, but they can also be estimated by maximum likelihood. Similarly, although we presented the ALMM as a single-depth model, it could readily be extended to multi-depth hierarchical approaches. The ALMM falls under

the unifying framework of compound Gaussian distributions, so it represents an extension to the family of dose models commonly used in OSL dating and is amenable to further development for sediments affected by post-depositional mixing in a variety of contexts.

Acknowledgements

This work was funded by the ARC Centre of Excellence for Australian Biodiversity and Heritage (CE170100015), an ARC Australian Laureate Fellowship (FL130100116) and the Monash Indigenous Studies Centre (Monash University). We thank Margaret Katherine, Wes Miller, Ray Whear and the Jawoyn Association Aboriginal Corporation for permission to collect samples at Nawarla Gabarnmang, and Yasaman Jafari and Terry Lachlan (University of Wollongong) for assisting with OSL sample preparation and measurement.

References

- Aandahl, Z., and L. Yates, 2023. rstanosl: OSL model fitting with Stan. R package version 1.0.0. <https://github.com/zaandahl/rstanosl>.
- Aitken, M. 1998. An Introduction to Optical Dating: The Dating of Quaternary Sediments by the Use of Photon-stimulated Luminescence. Oxford University Press, Oxford.
- Arnold, L., and R. Roberts. 2009. Stochastic modelling of multi-grain equivalent dose (D_e) distributions: Implications for OSL dating of sediment mixtures. *Quaternary Geochronology* **4**:204–230.
- Bateman, M. D., C. H. Boulter, A. S. Carr, C. D. Frederick, D. Peter, and M. Wilder. 2007. Detecting post-depositional sediment disturbance in sandy deposits using optical luminescence. *Quaternary Geochronology* **2**:57–64.
- Blaauw, M., and J. A. Christen. 2011. Flexible paleoclimate age-depth models using an autoregressive gamma process. *Bayesian Analysis* **6**:457–474.
- Bronk Ramsey, C. 2009. Bayesian Analysis of Radiocarbon Dates. *Radiocarbon* **51**:337–360.
- Bush, D., and J. Feathers. 2003. Application of OSL single-aliquot and single-grain dating to quartz from anthropogenic soil profiles in the SE United States. *Quaternary Science Reviews* **22**:1153–1159.
- Christophe, C., A. Philippe, G. Guérin, N. Mercier, and P. Guibert. 2018. Bayesian approach to OSL dating of poorly bleached sediment samples: Mixture Distribution Models for Dose (MD^2). *Radiation Measurements* **108**:59–73.
- Clarkson, C., Z. Jacobs, B. Marwick, R. Fullagar, L. Wallis, M. Smith, R. G. Roberts, E. Hayes, K. Lowe, X. Carah, S. A. Florin, J. McNeil, D. Cox, L. J. Arnold, Q. Hua, J. Huntley, H. E. A. Brand, T. Manne, A. Fairbairn, J. Shulmeister, L. Lyle, M. Salinas, M. Page, K. Connell, G. Park, K. Norman, T. Murphy, and C. Pardoe. 2017. Human occupation of northern Australia by 65,000 years ago. *Nature* **547**:306–310.
- Combès, B., A. Philippe, P. Lanos, N. Mercier, C. Tribolo, G. Guérin, P. Guibert, and C. Lahaye. 2015. A Bayesian central equivalent dose model for optically stimulated luminescence dating. *Quaternary Geochronology* **28**:62–70.
- David, B., B. Barker, F. Petchey, J.-J. Delannoy, J.-M. Geneste, C. Rowe, M. Eccleston, L. Lamb, and R. Whear. 2013. A 28,000 year old excavated painted rock from Nawarla Gabarnmang, northern Australia. *Journal of Archaeological Science* **40**:2493–2501.
- David, B., J.-J. Delannoy, J. Mialanes, C. Clarkson, F. Petchey, J.-M. Geneste, T. Manne, M. I. Bird, B. Barker, T. Richards, E. Chalmin, and G. Castets. 2019. 45,610–52,160 years of site and landscape occupation at Nawarla Gabarnmang, Arnhem Land plateau (northern Australia). *Quaternary Science Reviews* **215**:64–85.

- David, B., J.-M. Geneste, R. L. Whear, J.-J. Delannoy, M. Katherine, R. Gunn, C. Clarkson, H. Plisson, P. Lee, F. Petchey, C. Rowe, B. Barker, L. Lamb, W. Miller, S. Hoerlé, D. James, Élisabeth Boche, K. Aplin, I. J. McNiven, T. Richards, A. Fairbairn, and M. Jacqueline. 2011. Nawarla Gabarnmang, a $45,180 \pm 910$ cal BP Site in Jawoyn Country, Southwest Arnhem Land Plateau. *Australian Archaeology* **73**:73–77.
- Duller, G. 2003. Distinguishing quartz and feldspar in single grain luminescence measurements. *Radiation Measurements* **37**:161–165.
- Fu, X., A. A. Romanyukha, B. Li, N. R. Jankowski, T. J. Lachlan, Z. Jacobs, S. P. George, A. B. Rosenfeld, and R. G. Roberts. 2022. Beta dose heterogeneity in sediment samples measured using a Timepix pixelated detector and its implications for optical dating of individual mineral grains. *Quaternary Geochronology* **68**:101254.
- Gabry, J., D. Simpson, A. Vehtari, M. Betancourt, and A. Gelman. 2019. Visualization in Bayesian workflow. *Journal of the Royal Statistical Society: Series A (Statistics in Society)* **182**:389–402.
- Galbraith, R., and P. Green. 1990. Estimating the component ages in a finite mixture. *International Journal of Radiation Applications and Instrumentation. Part D. Nuclear Tracks and Radiation Measurements* **17**:197–206.
- Galbraith, R., and G. Laslett. 1993. Statistical models for mixed fission track ages. *Nuclear Tracks and Radiation Measurements* **21**:459–470.
- Galbraith, R., R. Roberts, and H. Yoshida. 2005. Error variation in OSL palaeodose estimates from single aliquots of quartz: a factorial experiment. *Radiation Measurements* **39**:289–307.
- Galbraith, R. F. 2005. *Statistics for Fission Track Analysis*. Chapman and Hall/CRC, Boca Raton.
- Galbraith, R. F., and R. G. Roberts. 2012. Statistical aspects of equivalent dose and error calculation and display in OSL dating: An overview and some recommendations. *Quaternary Geochronology* **11**:1–27.
- Galbraith, R. F., R. G. Roberts, G. M. Laslett, H. Yoshida, and J. M. Olley. 1999. Optical dating of single and multiple grains of quartz from Jinmium rock shelter, northern Australia: Part I, experimental design and statistical models. *Archaeometry* **41**:339–364.
- Gelman, A., J. B. Carlin, H. S. Stern, D. B. Dunson, A. Vehtari, and D. B. Rubin. 2013. *Bayesian Data Analysis*. Hardcover edition. Chapman and Hall/CRC.
- Gliganic, L. A., T. J. Cohen, M. Slack, and J. K. Feathers. 2016. Sediment mixing in aeolian sandsheets identified and quantified using single-grain optically stimulated luminescence. *Quaternary Geochronology* **32**:53–66.

- Guérin, G., C. Christophe, A. Philippe, A. S. Murray, K. J. Thomsen, C. Tribolo, P. Urbanova, M. Jain, P. Guibert, N. Mercier, S. Kreutzer, and C. Lahaye. 2017. Absorbed dose, equivalent dose, measured dose rates, and implications for OSL age estimates: Introducing the Average Dose Model. *Quaternary Geochronology* **41**:163–173.
- Heimsath, A. M., J. Chappell, N. A. Spooner, and D. G. Questiaux. 2002. Creeping soil. *Geology* **30**:111–114.
- Hoffman, M. D., and A. Gelman. 2014. The No-U-Turn Sampler: Adaptively Setting Path Lengths in Hamiltonian Monte Carlo. *Journal of Machine Learning Research* **15**:1593–1623.
- Hogg, A. G., T. J. Heaton, Q. Hua, J. G. Palmer, C. S. Turney, J. Southon, A. Bayliss, P. G. Blackwell, G. Boswijk, C. Bronk Ramsey, C. Pearson, F. Petchey, P. Reimer, R. Riemer, and L. Wacker. 2020. SHCal20 Southern Hemisphere Calibration, 0–55,000 Years cal BP. *Radiocarbon* **62**:759–778.
- Huntriss, A., 2008. A Bayesian Analysis of Luminescence Dating. Ph.D. thesis, Durham University.
- Jankowski, N. R., G. A. Gully, Z. Jacobs, R. G. Roberts, and G. J. Prideaux. 2016. A late Quaternary vertebrate deposit in Kudjal Yolgah Cave, south-western Australia: refining regional late Pleistocene extinctions. *Journal of Quaternary Science* **31**:538–550.
- Johnson, M. O., S. M. Mudd, B. Pillans, N. A. Spooner, L. Keith Fifield, M. J. Kirkby, and M. Gloor. 2014. Quantifying the rate and depth dependence of bioturbation based on optically-stimulated luminescence (OSL) dates and meteoric ^{10}Be . *Earth Surface Processes and Landforms* **39**:1188–1196.
- Li, B., Z. Jacobs, and R. G. Roberts. 2022. Bayesian analysis of D_e distributions in optical dating: Towards a robust method for dealing with outliers. *Quaternary Geochronology* **67**:101230.
- Mercier, N., J.-M. Galharret, C. Tribolo, S. Kreutzer, and A. Philippe. 2022. Luminescence age calculation through Bayesian convolution of equivalent dose and dose-rate distributions: the D_e - D_r model. *Geochronology* **4**:297–310.
- Merkle, E. C., D. Furr, and S. Rabe-Hesketh. 2019. Bayesian Comparison of Latent Variable Models: Conditional Versus Marginal Likelihoods. *Psychometrika* 2019 84:3 **84**:802–829.
- Murray, A., and A. Wintle. 2000. Luminescence dating of quartz using an improved single-aliquot regenerative-dose protocol. *Radiation Measurements* **32**:57–73.
- Norman, K., C. Shipton, S. O’Connor, W. Malanali, P. Collins, R. Wood, W. M. Saktura, R. G. Roberts, and Z. Jacobs. 2022. Human occupation of the Kimberley coast of northwest Australia 50,000 years ago. *Quaternary Science Reviews* **288**:107577.

- Olley, J. M., R. G. Roberts, H. Yoshida, and J. M. Bowler. 2006. Single-grain optical dating of grave-infill associated with human burials at Lake Mungo, Australia. *Quaternary Science Reviews* **25**:2469–2474.
- Peng, J., B. Li, and Z. Jacobs. 2020. Modelling heterogeneously bleached single-grain equivalent dose distributions: Implications for the reliability of burial dose determination. *Quaternary Geochronology* **60**:101108.
- Prescott, J., and J. Hutton. 1994. Cosmic ray contributions to dose rates for luminescence and ESR dating: Large depths and long-term time variations. *Radiation Measurements* **23**:497–500.
- Rink, W. J., J. S. Dunbar, W. R. Tschinkel, C. Kwapich, A. Repp, W. Stanton, and D. K. Thulman. 2013. Subterranean transport and deposition of quartz by ants in sandy sites relevant to age overestimation in optical luminescence dating. *Journal of Archaeological Science* **40**:2217–2226.
- Roberts, R., R. Galbraith, H. Yoshida, G. Laslett, and J. Olley. 2000. Distinguishing dose populations in sediment mixtures: a test of single-grain optical dating procedures using mixtures of laboratory-dosed quartz. *Radiation Measurements* **32**:459–465.
- Sivia, D. S., C. Burbidge, R. G. Roberts, and R. M. Bailey. 2004. A Bayesian Approach to the Evaluation of Equivalent Doses in Sediment Mixtures for Luminescence Dating. *AIP Conference Proceedings* **735**:305–311.
- Stan Development Team, 2022. RStan: the R interface to Stan. R package version 2.21.7. <https://mc-stan.org/>.
- Stockmann, U., B. Minasny, T. J. Pietsch, and A. B. McBratney. 2013. Quantifying processes of pedogenesis using optically stimulated luminescence. *European Journal of Soil Science* **64**:145–160.
- Vehtari, A., A. Gelman, and J. Gabry. 2017. Practical Bayesian model evaluation using leave-one-out cross-validation and WAIC. *Statistics and Computing* **27**:1413–1432.
- Vehtari, A., A. Gelman, D. Simpson, B. Carpenter, and P.-C. Bürkner. 2021. Rank-Normalization, Folding, and Localization: An Improved \hat{R} for Assessing Convergence of MCMC (with Discussion). *Bayesian Analysis* **16**:667–718.
- Wilkinson, M. T., P. J. Richards, and G. S. Humphreys. 2009. Breaking ground: Pedological, geological, and ecological implications of soil bioturbation. *Earth-Science Reviews* **97**:257–272.
- Wood, R., Z. Jacobs, D. Vannieuwenhuysse, J. Balme, S. O’Connor, and R. Whitau. 2016. Towards an Accurate and Precise Chronology for the Colonization of Australia: The Example of Riwi, Kimberley, Western Australia. *PLoS ONE* **11**:e0160123.
- Wood, S. N. 2003. Thin plate regression splines. *Journal of the Royal Statistical Society: Series B (Statistical Methodology)* **65**:95–114.

- Yackulic, C. B., M. Dodrill, M. Dzul, J. S. Sanderlin, and J. A. Reid. 2020. A need for speed in Bayesian population models: a practical guide to marginalizing and recovering discrete latent states. *Ecological Applications* **30**:e02112.
- Yates, L. A., Z. Aandahl, S. A. Richards, and B. W. Brook. 2022. Cross validation for model selection: A review with examples from ecology. *Ecological Monographs* **93**:e1557.
- Yates, L. A., S. A. Richards, and B. W. Brook. 2021. Parsimonious model selection using information theory: a modified selection rule. *Ecology* **102**:e03475.

A Appendix

A.1 Accounting for variation in dose rate with depth

For a sample of grains centred at equivalent dose $D = D_0 = \exp(d_0)$, the modelled age A is determined by the dose rate B using the rule

$$A = D/B, \quad (\text{A.12})$$

which we express in logged form as

$$a = d - b, \quad (\text{A.13})$$

where $a = \log(A)$, $b = \log(B)$, and $d = \log(D)$. The dose rates are determined by the environment and may vary with depth (i.e., $b = b(\text{depth})$). To investigate the consequences of grains (in a vertical mixing scenario) absorbing radiation energy at varying rates since their deposition, we model the sample distribution as an asymmetric Laplacian mixture on the log-age scale, rather than the log-dose scale. To implement this, we make the simplifying assumption that the mean dose rate for a (statistical) grain varies linearly on the log-dose scale in a region centred on the central (target) log-dose d_0 ; explicitly

$$b = b_0 + k(d - d_0), \quad (\text{A.14})$$

where k is the (unknown) slope of the linear trend. For example, grains that have migrated through deposits with lower dose rates than that of the final destination level will have a reduced mean dose rate—here we approximate these changes in mean dose rate by a linear trend on log-dose scale. The corresponding displacement-adjusted age of a statistical grain, with observed log-dose d_i , originating from the depth level with central log-dose d (ALMM marginalises over d), is given by

$$d_i - b_0 - k(d - d_0). \quad (\text{A.15})$$

The log-age mixture model can then be specified as

$$p(d_i | a_0, \tau, \eta, \sigma_0) = K \int_{-\infty}^{a_0} \exp\left(\frac{a - a_0}{\tau}\right) \exp\left(\frac{(d_i - b_0 - k(d - d_0) - a)^2}{-2\sigma_i^2}\right) da + \\ K \int_{a_0}^{\infty} \exp\left(\frac{a_0 - a}{\eta}\right) \exp\left(\frac{(d_i - b_0 - k(d - d_0) - a)^2}{-2\sigma_i^2}\right) da, \quad (\text{A.16})$$

where K is the normalisation constant. To compare with the original log-dose mixture, we change the variable of integration back to d using a formal change of variables, giving an

adjusted likelihood

$$p_{\text{adj}}(d_i | d_0, \tau', \eta', \sigma_0) = K(1 - k) \int_{-\infty}^{d_0} \exp\left(\frac{d - d_0}{\tau'}\right) \exp\left(\frac{(d_i - d)^2}{-2\sigma_i^2}\right) dd + K(1 - k) \int_{d_0}^{\infty} \exp\left(\frac{d_0 - d}{\eta'}\right) \exp\left(\frac{(d_i - d)^2}{-2\sigma_i^2}\right) dd, \quad (\text{A.17})$$

where $\tau' = \tau/(1 - k)$ and $\eta' = \eta/(1 - k)$ are rescaled rate parameters and $\frac{da}{dd} = 1 - k$. Thus, under the present modelling assumptions (i.e., local linearisation of the mean dose rate curve), the inclusion of changing dose rates in an ALMM log-age mixture does not change the estimates of d_0 (the parameter of interest). The absorption of the correction term suggests that the log-dose mixing parameters τ and η implicitly account for variation in several physical processes simultaneously, such as deposition rates, dose rates and vertical mixing rates.

A.2 Dirac delta functions

The Dirac delta function $\delta(t - t_0)$ is a generalised function defined by the integral

$$\int f(t)\delta(t - t_0)dt = f(t_0) \quad (\text{A.18})$$

for any continuous function f . It is often viewed informally as a ‘spike’ function satisfying

$$\delta(t - t_0) = \begin{cases} 0, & t \neq t_0 \\ \infty, & t = t_0. \end{cases} \quad (\text{A.19})$$

The definition can be extended to two dimensions such that

$$\delta(x - x_0, t - t_0) = \delta(x - x_0) \cdot \delta(t - t_0) \quad (\text{A.20})$$

satisfying

$$\int f(x, t)\delta(x - x_0, t - t_0)dxdt = f(x_0, t_0). \quad (\text{A.21})$$

In the context of compound probability distributions, using the Dirac delta function as the mixing distribution reduces the mixture to a single component characterised by the value t_0 (or x_0 and t_0 for the two-dimensional case).